Video Article

Magnetic Resonance Imaging Assessment of Carcinogen-induced Murine Bladder Tumors

Alexander P. Glaser[1], Daniele Procissi[2], Yanni Yu[3], Joshua J. Meeks[3]

[1]Department of Surgery, Division of Urology, NorthShore University HealthSystem

[2]Department of Radiology, Northwestern University Feinberg School of Medicine

[3]Department of Urology, Northwestern University Feinberg School of Medicine

Correspondence to: Joshua J. Meeks at joshua.meeks@northwestern.edu

URL: https://www.jove.com/video/59101
DOI: doi:10.3791/59101

Keywords: Urinary bladder neoplasms, magnetic resonance imaging, carcinogens, mice, BBN, bladder cancer

Date Published: 12/7/2018

Citation: Glaser, A.P., Procissi, D., Yu, Y., Meeks, J.J. Magnetic Resonance Imaging Assessment of Carcinogen-induced Murine Bladder Tumors. *J. Vis. Exp.* (), e59101, doi:10.3791/59101 (2018).

Abstract

Murine bladder tumor models are critical for the evaluation of new therapeutic options. Bladder tumors induced with the N-butyl-N-(4-hydroxybutyl) nitrosamine (BBN) carcinogen are advantageous over cell line-based models because they closely replicate the genomic profiles of human tumors, and, unlike cell models and xenografts, they provide a good opportunity for the study of immunotherapies. However, bladder tumor generation is heterogeneous; therefore, an accurate assessment of tumor burden is needed before randomization to experimental treatment. Described here is a BBN mouse model and protocol to evaluate bladder cancer tumor burden *in vivo* using a fast and reliable magnetic resonance (MR) sequence (true FISP). This method is simple and reliable because, unlike ultrasound, MR is operator-independent and allows for the straightforward post-acquisition image processing and review. Using axial images of the bladder, analysis of regions of interest along the bladder wall and tumor allow for the calculation of bladder wall and tumor area. This measurement correlates with *ex vivo* bladder weight (r_s= 0.37, p = 0.009) and tumor stage (p = 0.0003). In conclusion, BBN generates heterogeneous tumors that are ideal for evaluation of immunotherapies, and MRI can quickly and reliably assess tumor burden prior to randomization to experimental treatment arms.

Introduction

Bladder cancer is the fifth most common cancer overall, responsible for approximately 80,000 new cases and 16,000 deaths in the United States in 2017[1]. After about 30 years without significant advances in the systemic treatment of bladder cancer[2], recent anti-PD-1 and anti-PD-L1 checkpoint inhibitor trials have demonstrated exciting and occasionally durable responses in patients with advanced urothelial carcinoma[3,4,5]. However, only approximately 20% of patients show an objective response to these treatments, and further studies are needed to expand the effective use of immunotherapy in patients with bladder cancer.

Murine bladder cancer models are critical tools in preclinical evaluation of novel treatments[6,7]. In order to control for tumor size when randomizing mice to different treatments, tumor burden must be assessed and controlled between treatment groups. Previous studies have used ultrasound or bioluminescence to evaluate orthotopic cell line-based bladder cancer models[8,9,10,11]. However, both techniques present several disadvantages. Ultrasound measurements can be influenced by skills of the operator and lack three-dimensional features and high spatial resolution. Bioluminescence methods can only provide semi-quantitative evaluation of the tumor cells and do not allow for visualization of bladder anatomy and morphology. Furthermore, bioluminescence can only be used with cell line-based models, which express bioluminescent genes in hairless mice or mice with white coats.

Magnetic resonance imaging (MRI), on the other hand, offers unique flexibility in the acquisition of high-resolution anatomical images, exhibiting a broad range of tissue contrast that enables accurate visualization and quantitative assessment of tumor burden without the need to express bioluminescent properties. MR images are more easily reproducible with the appropriate analysis pipelines and guaranteed 3-D visualization of the bladder. The biggest limitations of MRI are the length of time necessary for an examination and associated high costs that limit high throughput assays. However, several studies have shown that MR sequences can provide high-quality diagnostic images that can be used to effectively detect and monitor cell line-based bladder tumors; thus, they may be used for high throughput analysis[9,12].

Here, we describe a non-invasive MR-based method to reliably and efficiently characterize carcinogen-induced bladder tumors in mice. To accomplish this, we use a fast imaging with steady state precession MR technique (true FISP), which guarantees short scanning sessions while still providing high quality and high spatial resolution (~100 microns) for the detection and measurement of bladder tumors[13]. Furthermore, to confirm the accuracy of this non-invasive MRI assay, we describe the correlation between MRI-derived parameters and *ex vivo* bladder weight as well as pathologically-confirmed tumor stage.

Protocol

All methods described here have been approved by the Institutional Animal Care and Use Committee (IACUC) of Northwestern University.

1. Induction of tumors with BBN

1. Obtain male C57/BL6 mice, each at least 6 weeks old.
   NOTE: Male mice develop bladder cancer more quickly and consistently than female mice[14,15].
2. Add N-nitrosobutyl(4-hydroxybutyl) amine (BBN) at a dose of 0.05% to the drinking water. Store it in an opaque container and provide it *ad libitum* as drinking water to mice[16].
   NOTE: Storing the BBN solution in a clear container will degrade the carcinogen[17].
3. Change the 0.05% BBN water twice per week.
4. Monitor the animals by inspecting for signs of distress associated with bladder tumors including hematuria, firm bladder, and masses. Inspect the mice twice per week or in accordance with local IACUC guidelines.
5. Expect the tumors to develop between 16 and 24 weeks of exposure[18].

2. MRI setup

1. Perform a subcutaneous injection of sterile saline (0.1–0.2 mL using a 25–27 G needle and 1 mL syringe) 10 min prior to MRI to facilitate bladder filling.
2. Anesthetize each mouse with a gas mixture of 100% O_2 and isoflurane (2%–4% as necessary). Verify an adequate plane of anesthesia by testing the withdrawal reflex (toe pinch) before proceeding.
3. Transfer the mouse to the imaging holder outfitted with a nosecone for delivery of inhaled isoflurane (0.5%–3%).
4. Monitor body temperature and respiration using a rectal temperature probe connected to the physiological recording computer.
   NOTE: Normal body temperature (36–37 °C) is maintained using the recirculating hot water circuit built into the animal MR holder. Temperature is measured through a rectal sensor and recorded on the physiological monitoring computer using dedicated physiological monitoring software. The same system is used to record the respiration and electrocardiogram signals measured through a pneumatic pillow placed under the rib cage and *via* 3-lead electrocardiogram electrodes. The respiration signal is also used for triggering MRI acquisition and reducing artifacts associated with respiration motion.

3. MRI image acquisition

1. Utilize a quadrature body coil for excitation.
2. Place a 4-channel receiver coil on the lower abdomen of the mouse being scanned to enable optimized detection of signals from the region of interest.
3. Initiate automatic adjustments through the integrated imaging software to acquire a tri-axial set of images of the whole mouse body. From this reference set of images, identify the region of interest (in this case, the bladder region).
4. Acquire three sets of orthogonal-sliced images along the axial, coronal, and sagittal planes using radiological frames of reference.
5. Utilize the true FISP imaging sequence (included as one of the features in the integrated imaging software) with the following MR parameters: TR = 900 msec, TE = 2 ms, FA = 70, 14 averages.
   NOTE: This set of parameters allows for rapid imaging with high diagnostic quality, including T1/T2 weighting in <10 min per mouse.
6. Spatial resolution and slice thickness are determined by geometric parameters selected by the user through the graphical interface of the integrated imaging platform. This results in a series of slices across the whole bladder of 0.5 mm thickness with an in-plane resolution of 0.148 mm.

4. MR image analysis

1. Identify the set of slices of 0.5 mm thickness and in-plane resolution of 0.148 mm covering the whole bladder.
2. Export to the medical image analysis software by selecting the folder with corresponding images in ANALYZE format.
3. Select “representative axial view” at the center of the bladder for quantitative analysis by scrolling through the generated images and identifying a slice at the midpoint of the bladder, which allows for visualization of the bladder wall and lumen.
   NOTE: The center slice should be the chosen one with the largest diameter.
4. Carefully delineate the region of interest (ROI) by manually tracing the boundaries around the outer edge of the bladder (BLA_{out}) and around the inner lumen (BLA_{in}) of the bladder (see schematic and representative figures in **Figure 2**) in the selected representative axial view.
5. Subtract the inner lumen from the outer edge to calculate the surface area of the bladder wall.
   $BLA_{wall} = BLA_{out} - BLA_{in}$
   NOTE: The surface area of a control bladder with no tumor is expected to be less than that with a bladder tumor.

5. Euthanasia and dissection of bladder

1. After 20 weeks of BBN exposure, euthanize the mice using standard operating procedures in accordance with local IACUC guidelines.
2. Clean the area of incision with 70% ethanol, then grasp and lift the abdominal wall skin with forceps.
3. Make a midline incision from the pubic symphysis to the xiphoid process.
4. Sharply incise the peritoneal cavity by grasping with forceps and incising with scissors.
5. Identify the bladder, which is located in the midline lower abdomen.
6. Identify and cut the median umbilical ligament connecting the dome of the bladder to the umbilicus and abdominal wall.
7. Grasp the dome of the bladder with forceps to provide countertraction and dissect the bladder away from surrounding structures, including the seminal vesicles, rectum, and fat.
8. Identify the ureters entering the bladder and cut with scissors close to the bladder.
9. Lifting the bladder cephalad, cut the urethra with scissors and remove the bladder.

10. Immediately weigh the bladder after rinsing it with PBS.

6. Histologic examination of bladder tissue

1. Fix the bladder tissue in 10% neutral buffered formalin for 36–48 h at room temperature (RT).
2. Embed the tissue in paraffin blocks, cut the slides for subsequent examination, and stain the slides with hematoxylin and eosin for microscopic examination as described previously[19,20].
3. Perform a microscopic examination of the mouse bladder at low (2.5x and 10x) and high (20x and 40x) magnifications, examining for macroscopic lesions, hyperplasia, carcinoma *in situ*, papillomas, papillary tumors, and invasive neoplasms[19,21].

Representative Results

Using the protocol described (**Figure 1**), bladder tumors were induced in C57/B6 male mice. MRI was performed at 16 weeks, and mice were euthanized at 20 weeks. *Ex vivo* bladder weights (BW) for each mouse were recorded. Slides were stained with hematoxylin and eosin, and all histology slides were reviewed for tumor stage.

To analyze the tumor burden using MR, the bladder wall inner lumen (BLA_{in}) was subtracted from the bladder wall outer lumen (BLA_{out}) to calculate the thickness of the bladder wall (BLA_{wall}) (**Figure 2**). Representative true FISP MR images, bladder wall 3-D reconstructions, and pathologic images of a control mouse (i.e., no tumor) are shown in **Figure 3A**-**F,** and a mouse with a large tumor is shown in **Figure 3G**-**L**.

The MRI-derived parameter BLA_{wall} correlates weakly with *ex vivo* BW (r_s = 0.37, p = 0.009; **Figure 4**). Examination of the MRI-derived BLA_{wall} parameter and BW data demonstrates an association with tumor stage (Kruskal-Wallis test MRI p = 0.0003, **Figure 5A**; BW p = 0.0006; **Figure 5B**), as well as an association when stratifying pathology by non-muscle-invasive bladder cancer and muscle-invasive bladder cancer (Mann-Whitney U test MRI p = 0.0002, **Figure 5C**; BW p < 0.0001, **Figure 5D**). The performance of BLA_{wall} and BW to determine muscle-invasive bladder cancer is shown in **Figure 5E**. The area under the curve (AUC) for BLA_{wall} (AUC = 0.81, 95% CI 0.68-093) is statistically similar to AUC for BW (AUC = 0.89, 95% CI 0.80-0.98; p = 0.30).

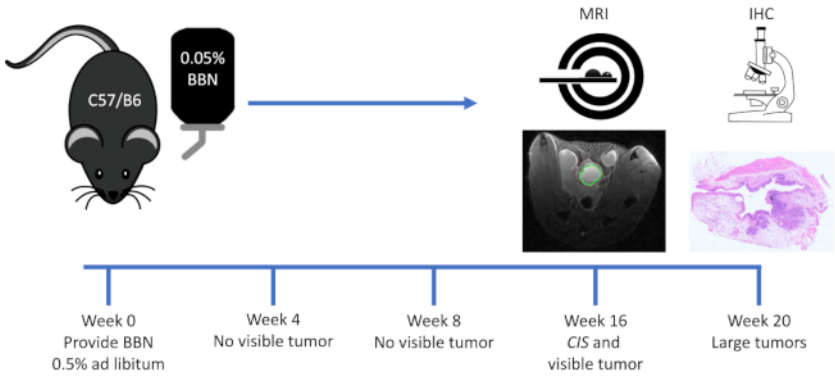

Figure 1: Schema for bladder tumor induction with BBN and timing of MRI and euthanasia. BBN is administered *ad libitum* at a concentration of 0.05% in drinking water. Mice undergo MRI at 16 weeks. Mice are euthanized at 20 weeks and bladders of each are examined with immunohistochemistry. Please click here to view a larger version of this figure.

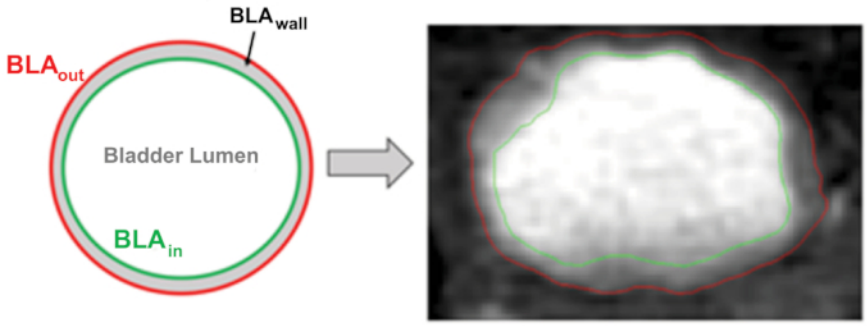

Figure 2: Schematic graphical depiction of method to obtain BLA_{wall} and representative MR image with corresponding outlines. Using intensity of MRI images, the outer wall of a bladder was identified and an outline was drawn in red (BLA_{out}). The hyperintense bladder lumen was outlined in green (BLA_{in}), and the corresponding bladder lumen area was obtained. Subtraction of these two quantities yielded the BLA_{wall} parameter, which corresponds to the light gray disk in the graphical image. Please click here to view a larger version of this figure.

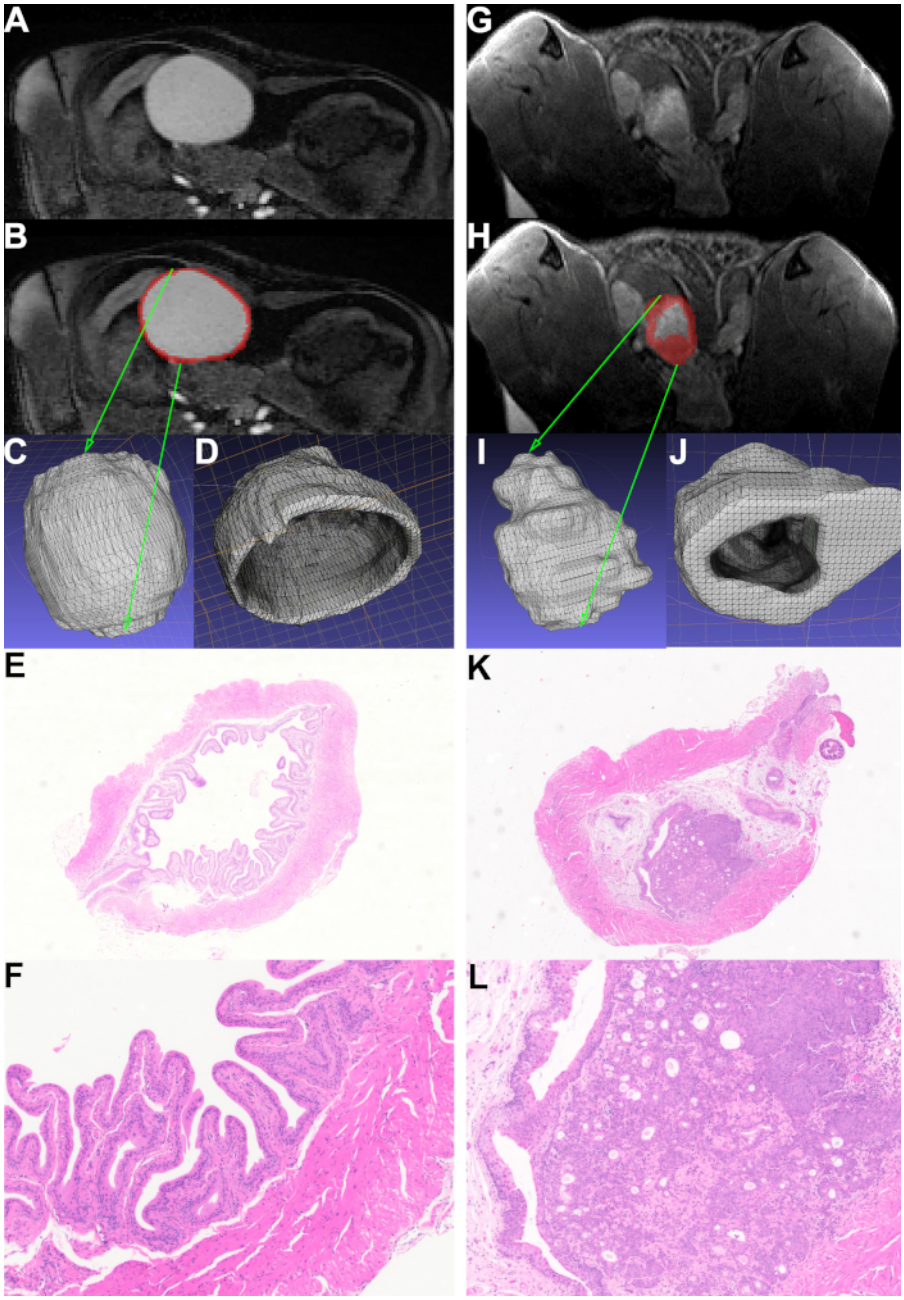

Figure 3: Representative true FISP MR images, bladder wall 3-D reconstructions, and pathologic images of a control mouse (i.e., no tumor) (A-F)and a mouse with a large tumor (G-L). (A) Representative MR image of a mouse with no tumor. **(B)** Segmentation of bladder wall area (BLA_{wall}), outlined in red, defined as the area between the bladder lumen (BLA_{in}) and outer bladder wall (BLA_{out}). **(C)** 3-D rendering of the bladder wall from a control mouse, generated by defining BLA_{wall} at every slice through the bladder. Green arrows illustrate the bladder on a 2-D image translated to 3-D rendering. **(D)** 3-D rendering of a cut-out of BLA_{wall} from a control mouse. **(E)** Low power (2.5x) and **(F)** high power (10x) images of the same mouse bladder. **(G)** Representative MR image of a mouse with a large tumor. **(H)** Segmentation of bladder wall area (BLA_{wall}), outlined in red, defined as the area between the bladder lumen (BLA_{in}) and outer bladder wall (BLA_{out}). **(I)** 3-D rendering of the bladder wall of a mouse with a large tumor. **(J)** 3-D rendering of a cut-out of the bladder of a mouse with a large tumor, generated by defining BLA_{wall} at every slice through the bladder. Green arrows illustrate the bladder on a 2-D image translated to 3-D rendering. **(K)** Low power (2.5x) and **(L)** high power (10x) images of the same mouse bladder. Please click here to view a larger version of this figure.

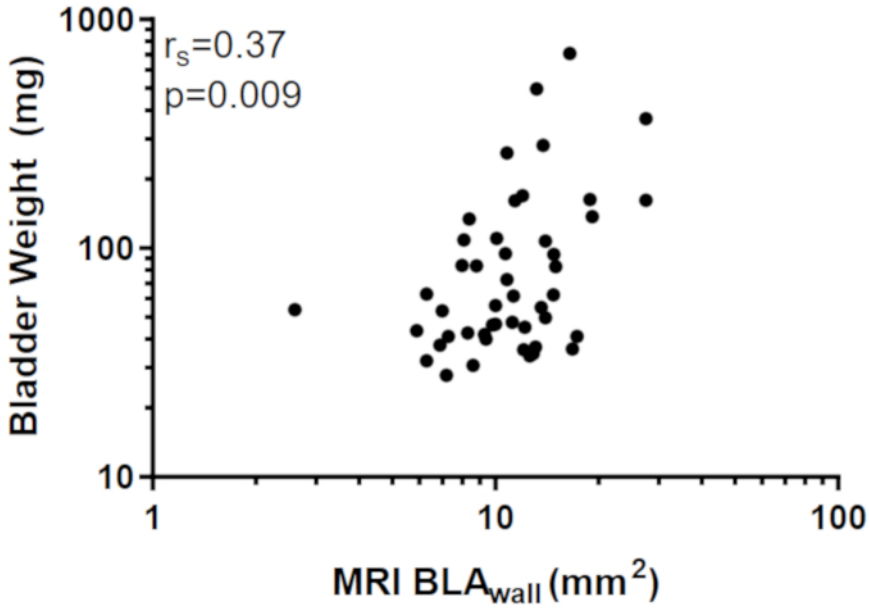

Figure 4: Spearman correlation between the MRI-derived BLA_{wall} and final bladder weight. Please click here to view a larger version of this figure.

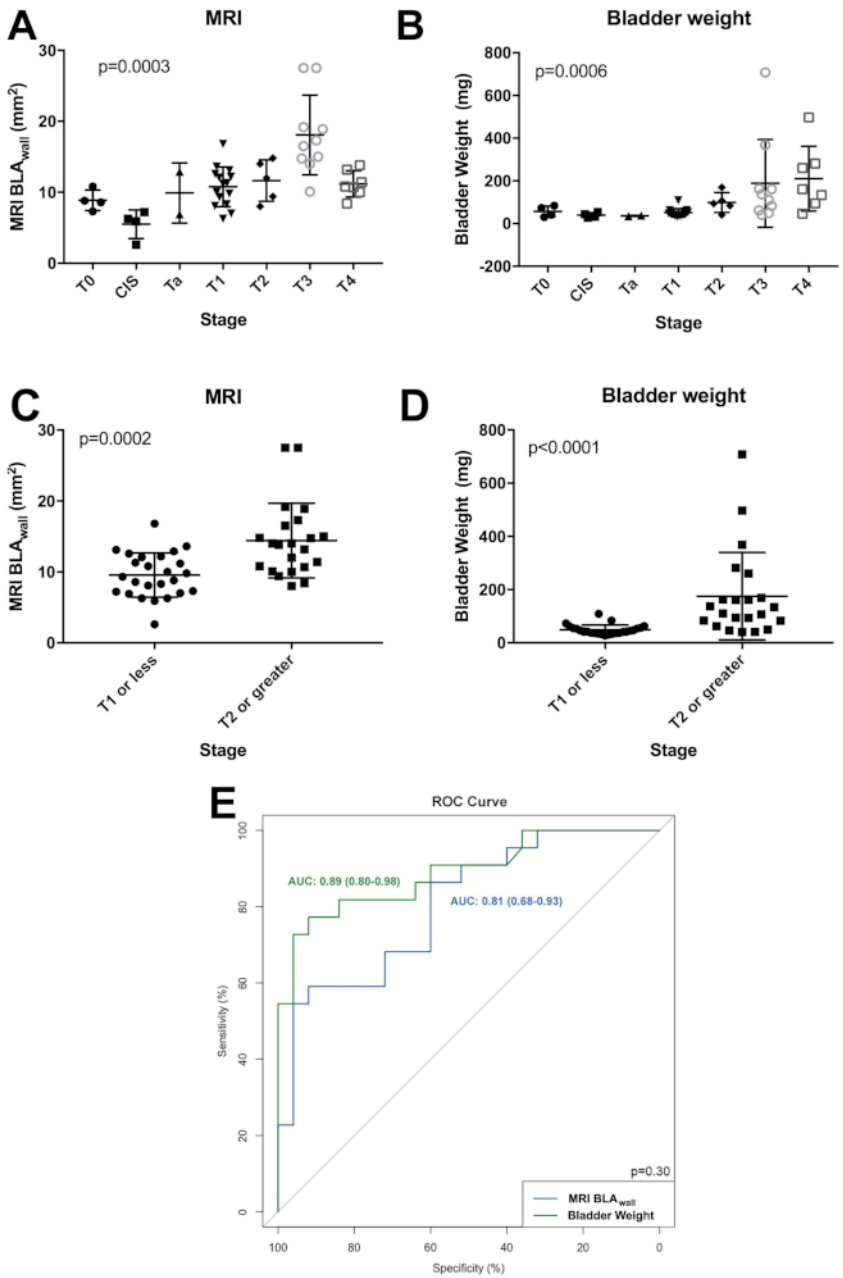

Figure 5: Comparisons of pathologic stage and MRI-derived parameter BLA$_{wall}$ in 47 mice. (A) Comparison of all pathologic stages and MRI BLA$_{wall}$ (Kruskal-Wallis test).**(B)** Comparison of all pathologic stages and bladder weight (Kruskal-Wallis test). **(C)** Comparison of non-muscle-invasive bladder cancer (stage ≤T1) and muscle-invasive bladder cancer (stage ≥T2) with MRI BLA$_{wall}$ (Mann-Whitney U test). **(D)** Comparison of non-muscle-invasive bladder cancer (stage ≤T1) and muscle-invasive bladder cancer (stage ≥T2) with bladder weight (Mann-Whitney U test). **(E)** ROC curve of the MRI-derived bladder area and final bladder weight in determining muscle-invasive bladder cancer (stage ≥T2). The listed p-value is the difference between the two AUCs. Please click here to view a larger version of this figure.

Discussion

Accurate imaging of tumor models is necessary for appropriate pre-euthanasia staging and animal randomization prior to initiation of experimental treatment. Using the procedure presented here, we demonstrate methodology to (1) generate bladder tumors using the BBN carcinogen and (2) stratify bladder tumor burden through the use of MR. An MR-derived area measurement (BLA$_{wall}$) correlates significantly with *ex vivo* bladder weight and is associated with pathologic tumor stage.

By adopting a rapid imaging approach with short acquisition times at high spatial resolution (true FISP) and high diagnostic quality, we can conduct high throughput assays of mice at intermediate stages of tumor development, prior to treatment randomization. Our report is consistent

with prior reports of MR imaging of cell line-based tumor implants[9,12] and confirms its potential as a tool to optimize large subject number drug studies.

In this MRI protocol, it is critical to image the mouse with a full bladder to obtain high quality images and delineate the differences between the tumor and bladder lumen. We find that injecting each mouse with saline 10 minutes before imaging allows for adequate imaging of the bladder. Further critical steps include reliable triggering of MRI acquisition using the respiration signal detected with a pneumatic pillow placed under the mouse rib cage and acquisition of an adequate number of MR slices that enables coverage of the whole bladder.

Other options for imaging development and progression of murine bladder tumors include ultrasound[8] and bioluminescence[10,11]. Micro-ultrasound imaging of implanted MBT-2 cells detected tumors in 15 mice, 13 of which were histologically confirmed to have tumors[8]. Ultrasound volume correlated significantly with stereoscopic volume of tumor, but tumor weight and stage were not investigated[8]. Bioluminescence has been used to accurately monitor cell line-based tumor implants, but it cannot be used to monitor carcinogen-induced cancers without transplanting carcinogen-derived tumors from one mouse to another. The ability to accurately monitor carcinogen-induced cancers is critical, as these models have several advantages over cell line models. Cell line-based models are genetically homogenous and derived from tumors that have already evaded immunosurveillance, and implanted tumors grow rapidly without a chronic inflammatory microenvironment[22]. The BBN model has been used successfully for over 30 years, and it remains a critical model for the understanding of bladder cancer development and treatment[23,24,25]. Furthermore, the BBN model demonstrates mutational and gene expression profiles similar to human bladder cancer, while still retaining the intact immune system to allow for the study of potential immunotherapeutic agents[26,27].

Availability of dedicated small animal MRIs as shared resources at multiple institutions makes this techniques advantageous and practical for basic research and screening of novel therapies. However, there are some limitations. Mice were imaged only at one timepoint, not continuously during the development of tumors. However, based on our statistical results, we suggest that the single timepoint value is able to accurately stratify mice into groups by tumor size and stage, and it represents an ideal, non-invasive parameter to classify and assign subjects to different groups. Multiple tumor stages were generated using BBN, ranging from Ta to T4. However, these may be stratified (as suggested in **Figure 5C-D**) as muscle-invasive (T2 or greater) and non-muscle invasive (T1 or less), as this is standard management in human bladder cancer[28].

Another potential limitation is that the BLA_{wall} parameter was derived using a single slice through each bladder and not all available slices covering it. These criteria were chosen to reduce analysis pipeline requirements (i.e., requirement of drawing multiple ROIs across multiple slices) and were deemed sufficient for a fast, quantitative assay. More complex volumetric analysis can be conducted on the subjects (i.e., shown for illustrative purposes in **Figure 3**) but would inevitably require more effort and costs. Automated image processing algorithms can be used for automatic delineation of bladder region; however, these methods suffer from intrinsic variability of bladder shape and size among individual mice and require significant testing and validation prior to reliable adoption in a preclinical study[29].

Qualitative assessment of volumetric data suggest that this single slice method is sufficient for this type of assay. However, it is possible that more advanced assays may require this additional data/image processing step. From the acquisition point of view, there are several additional scans that could be acquired, which may further increase the ability to predict progression of tumors while also revealing more subtle tumor microenvironment changes. These additional techniques include dynamic contrast enhanced MRI, diffusion weighted MRI, and other sequences[30] that enable a comprehensive, multi-parametric characterization of the bladder wall. However, consideration of cost and efficiency led us to confine our assay to the one described in this protocol.

In conclusion, we describe the methodology for T1/T2-weighted rapid imaging MR sequences (true FISP) to acquire multi-slice images covering the entire mouse bladder. We demonstrate that these images can be used to determine the extent of tumor in a carcinogen-based model of murine bladder cancer. MRI data correlates with bladder tissue weights and is associated with tumor stage. These results support the use of this fast and reliable MRI assay to stratify mice prior to experimental treatment randomization.

Disclosures

The authors have nothing to disclose.

Acknowledgements

J. J. M. is funded by the Veterans Health Administration Merit grant BX0033692-01. J. J. M. is also supported by the John P. Hanson Foundation for Cancer Research at the Robert H. Lurie Comprehensive Cancer Center of Northwestern University. We thank the Center for Translational Imaging for providing the MRI acquisition and processing. Funding sources had no role in writing of the manuscript or the decision to submit for publication.

References

1. Siegel, R. L., Miller, K. D., Jemal, A. Cancer Statistics, 2017. *CA: A Cancer Journal for Clinicians.* **67** (1), 7-30 (2017).
2. Abdollah, F. *et al.* Incidence, survival and mortality rates of stage-specific bladder cancer in United States: a trend analysis. *Cancer Epidemiology.* **37** (3), 219-225 (2013).
3. Rosenberg, J. E. *et al.* Atezolizumab in patients with locally advanced and metastatic urothelial carcinoma who have progressed following treatment with platinum-based chemotherapy: a single-arm, multicentre, phase 2 trial. *The Lancet.* **387** (10031), 1909-1920 (2016).
4. Sharma, P. *et al.* Nivolumab monotherapy in recurrent metastatic urothelial carcinoma (CheckMate 032): a multicentre, open-label, two-stage, multi-arm, phase 1/2 trial. *The Lancet Oncology.* **17** (11), 1590-1598 (2016).
5. Bellmunt, J. *et al.* Pembrolizumab as Second-Line Therapy for Advanced Urothelial Carcinoma. *New England Journal of Medicine.* **376** (11), 1015-1026 (2017).

6. Chan, E., Patel, A., Heston, W., Larchian, W. Mouse orthotopic models for bladder cancer research. *BJU International.* **104** (9), 1286-1291 (2009).
7. Zhang, N., Li, D., Shao, J., Wang, X. Animal models for bladder cancer: The model establishment and evaluation (Review). *Oncology Letters.* **9** (4), 1515-1519 (2015).
8. Patel, A. R. *et al.* Transabdominal micro-ultrasound imaging of bladder cancer in a mouse model: a validation study. *Urology.* **75** (4), 799-804 (2010).
9. Chin, J., Kadhim, S., Garcia, B., Kim, Y. S., Karlik, S. Magnetic resonance imaging for detecting and treatment monitoring of orthotopic murine bladder tumor implants. *The Journal of Urology.* **145** (6), 1297-1301 (1991).
10. Jurczok, A., Fornara, P., Soling, A. Bioluminescence imaging to monitor bladder cancer cell adhesion in vivo: a new approach to optimize a syngeneic, orthotopic, murine bladder cancer model. *BJU International.* **101** (1), 120-124 (2008).
11. Vandeveer, A. J. *et al.* Systemic Immunotherapy of Non-Muscle Invasive Mouse Bladder Cancer with Avelumab, an Anti-PD-L1 Immune Checkpoint Inhibitor. *Cancer Immunology Research.* **4** (5), 452-462 (2016).
12. Kikuchi, E. *et al.* Detection and quantitative analysis of early stage orthotopic murine bladder tumor using in vivo magnetic resonance imaging. *Journal of Urology.* **170** (4 Pt 1), 1375-1378 (2003).
13. Chung, H. W. *et al.* T2-weighted fast MR imaging with true FISP versus HASTE: comparative efficacy in the evaluation of normal fetal brain maturation. *American Journal of Roentgenology.* **175** (5), 1375-1380 (2000).
14. Miyamoto, H. *et al.* Promotion of bladder cancer development and progression by androgen receptor signals. *Journal of the National Cancer Institute.* **99** (7), 558-568 (2007).
15. Bertram, J. S., Craig, A. W. Specific induction of bladder cancer in mice by butyl-(4-hydroxybutyl)-nitrosamine and the effects of hormonal modifications on the sex difference in response. *European Journal of Cancer.* **8** (6), 587-594 (1972).
16. Nagao, M. *et al.* Mutagenicity of N-butyl-N-(4-hydroxybutyl)nitrosamine, a bladder carcinogen, and related compounds. *Cancer Research.* **37,** 399-407 (1977).
17. Hirose, M., Fukushima, S., Hananouchi, M., Shirai, T., Ogiso, T. Different susceptibilities of the urinary bladder epithelium of animal species to three nitroso compounds. *Gan. Gann; The Japanese Journal of Cancer Research.* **67** (2), 175-189 (1976).
18. Shin, K. *et al.* Cellular origin of bladder neoplasia and tissue dynamics of its progression to invasive carcinoma. *Nature Cell Biology.* **16** (5), 469-478 (2014).
19. Epstein, J. I. *Immunohistology of the Bladder, Kidney, and Testis.* Diagnostic Immunohistochemistry, Fifth Edition. Chapter 17, 624-661 (2019).
20. Cohen, S. M., Ohnishi, T., Clark, N. M., He, J., Arnold, L. L. Investigations of rodent urinary bladder carcinogens: collection, processing, and evaluation of urine and bladders. *Toxicologic Pathology.* **35** (3), 337-347 (2007).
21. Wood, D. P. Jr. *Tumors of the bladder.* Campbell-Walsh Urology. **11** (92), 2184-2204 (2016).
22. Zitvogel, L., Pitt, J. M., Daillere, R., Smyth, M. J., Kroemer, G. Mouse models in oncoimmunology. *Nature Reviews Cancer.* (2016).
23. Kaneko, S., Li, X. X chromosome protects against bladder cancer in females via a KDM6A-dependent epigenetic mechanism. *Science Advances.* **4** (6), eaar5598 (2018).
24. Smilowitz, H. M. *et al.* Biodistribution of gold nanoparticles in BBN-induced muscle-invasive bladder cancer in mice. *International Journal of Nanomedicine.* **12,** 7937-7946 (2017).
25. Dai, Y. C. *et al.* The interaction of arsenic and N-butyl-N-(4-hydroxybutyl)nitrosamine on urothelial carcinogenesis in mice. *PLoS One.* **12** (10), e0186214 (2017).
26. Williams, P. D., Lee, J. K., Theodorescu, D. Molecular Credentialing of Rodent Bladder Carcinogenesis Models. *Neoplasia.* **10** (8), 838-IN821 (2008).
27. Fantini, D. *et al.* A Carcinogen-induced mouse model recapitulates the molecular alterations of human muscle invasive bladder cancer. *Oncogene.* **37** (14), 1911-1925 (2018).
28. Network, N. C. C. *NCCN Guidelines in Clinical Oncology - Bladder Cancer 5.2018.*, <https://www.nccn.org/professionals/physician_gls/pdf/bladder.pdf> (2018).
29. Costa, M. J., Delingette, H., Novellas, S., Ayache, N. Automatic segmentation of bladder and prostate using coupled 3-D deformable models. *Medical Image Computing and Computer-Assisted Intervention.* **10** (Pt 1), 252-260 (2007).
30. Rosenkrantz, A. B. *et al.* Utility of quantitative MRI metrics for assessment of stage and grade of urothelial carcinoma of the bladder: preliminary results. *American Journal of Roentgenology.* **201** (6), 1254-1259 (2013).

